

Van der Waals engineering of ultrafast carrier dynamics in magnetic heterostructures

Paulina Majchrzak,[†] Klara Volckaert,[†] Deepnarayan Biswas,[†] Denny Puntel,[‡]
Wibke Bronsch,[¶] Federico Cilento,[¶] Xing-Chen Pan,[§] Yong P. Chen,^{†,§,||} and
Søren Ulstrup^{*,†}

[†]*Department of Physics and Astronomy, Interdisciplinary Nanoscience Center, Aarhus University, 8000 Aarhus C, Denmark*

[‡]*Dipartimento di Fisica, Università degli Studi di Trieste, 34127 Trieste, Italy*

[¶]*Elettra - Sincrotrone Trieste S.C.p.A., 34149 Basovizza, Italy*

[§]*Advanced Institute for Materials Research, Tohoku University, Sendai 980-8577, Japan*

^{||}*Department of Physics and Astronomy and School of Electrical and Computer Engineering and Purdue Quantum Science and Engineering Institute, Purdue University, West Lafayette, IN 47907, USA*

Abstract

Heterostructures composed of the intrinsic magnetic topological insulator MnBi_2Te_4 and its non-magnetic counterpart Bi_2Te_3 host distinct surface band structures depending on the stacking order and exposed termination, allowing fine control of their magnetic, electronic and optical properties. Here, we probe the ultrafast dynamical response of MnBi_2Te_4 and MnBi_4Te_7 following near-infrared optical excitation using time- and angle-resolved photoemission spectroscopy. We gain access to the out-of-equilibrium surface electronic structure of both MnBi_2Te_4 and Bi_2Te_3 surface terminations of MnBi_4Te_7 , revealing an instantaneous occupation of states that are resonant with the optical excitation in the Bi_2Te_3 layer followed by carrier extraction into the adjacent MnBi_2Te_4 layers with a laser fluence-tunable delay of up to 350 fs. The ensuing thermal relaxation processes are driven by in-plane phonon scattering with significantly slower relaxation times in the magnetic MnBi_2Te_4 septuple layers. The competition of interlayer charge transfer and intralayer phonon scattering establishes MnBi_2Te_4 -based compounds as a platform for controlling ultrafast charge transfer processes in combination with magnetism and topology in van der Waals heterostructures.

KEYWORDS: Magnetic topological insulators, MnBi_2Te_4 , van der Waals heterostructures, ultrafast carrier dynamics, time- and angle-resolved photoemission spectroscopy.

Heterojunctions composed of two-dimensional (2D) semiconducting materials are highly promising for developing novel optoelectronic devices due to tunable band gaps and charge carrier dynamics.¹ The interplay of charge and phonon interactions has been intensively examined in transition metal dichalcogenide heterostructures, unveiling sub 50-fs interlayer carrier extraction that is ideal for light harvesting and photovoltaics.^{2,3} Van der Waals compounds based on the antiferromagnetic topological insulator MnBi_2Te_4 present another attractive candidate for advanced opto- and spintronics applications due to the realization of exotic phases such as the quantum anomalous Hall effect⁴ and axion electrodynamics.⁵ Yet, optically-induced ultrafast carrier dynamics and charge transfer processes in these materi-

als remain largely unexplored. Moreover, the properties of these materials can be elegantly engineered via van der Waals stacking. For example, combining a quintuple layer (QL) of the non-magnetic topological insulator Bi_2Te_3 with a septuple layer (SL) of MnBi_2Te_4 reduces the antiferromagnetic exchange interaction between neighbouring planes of Mn atoms, while strengthening the affinity of the system to undergo a spin-flop transition to ferromagnetic order.⁶ As a result, van der Waals heterostructures of the form $\text{MnBi}_2\text{Te}_4(\text{Bi}_2\text{Te}_3)_m$ ($m = 1, 2, 3, \dots$) offer a platform for tuning the magnetic properties^{7,8} as well as accessing topological magnetotransport⁹ and the quantum anomalous/spin Hall effects.^{10,11}

In order to gain access to the energy- and momentum-resolved ultrafast carrier dynamics of $\text{MnBi}_2\text{Te}_4(\text{Bi}_2\text{Te}_3)_m$ heterostructures, we employ time- and angle-resolved photoemission spectroscopy (TR-ARPES). This approach utilizes a near-infrared optical excitation to induce direct optical transitions from the occupied to the unoccupied states. The out-of-equilibrium electronic band structure of the excited state is then measured by a time-delayed ultraviolet probe pulse, giving direct insights into charge transfer processes and phonon relaxation between bulk and surface states on a given heterostructure termination.¹² This approach has revealed thermal dynamics with a duration of 4 ps in MnBi_2Te_4 across the magnetic ordering temperature,¹³ as well as photoinduced filling of the surface state hybridization gap of the QL termination in a heterostructure with stoichiometry $m = 3$.¹⁴ Here, we determine how carrier extraction and relaxation is controlled by the balance of inter- and intralayer interactions by comparing the time-dependent evolution of excited electronic states between the $m = 0$ and $m = 1$ heterostructures, i.e. MnBi_2Te_4 and MnBi_4Te_7 . We find that carriers are instantaneously excited in the QL of MnBi_4Te_7 and are then gradually extracted into the SL with a fluence-dependent delay of up to 350 fs. Thermal relaxation then proceeds at a slower rate within the magnetic SL layer, implying that the layer-dependent electronic and magnetic properties can be optically controlled on an ultrafast timescale.

The MnBi_2Te_4 and MnBi_4Te_7 crystals were grown by the flux method. High purity Mn, Bi, and Te powders were sealed in quartz tubes with a ratio of Mn:Bi:Te = 1:10:16. The tubes

were heated to 900°C and then cooled to 595/590°C, respectively. The flux was removed by centrifuging after cooling. Our TR-ARPES measurements were performed at the T-ReX facility (Trieste, Italy). Pump and probe pulses were generated by a 250 kHz Ti:sapphire Coherent Reg A laser system, whose output was centered at an energy of 1.55 eV. The fourth harmonic (6.2 eV) of the fundamental beam was used as an *s*-polarised probe pulse. The remainder of the beam was used as a *p*-polarised pump with a tunable fluence in the range of 40-280 $\mu\text{J}/\text{cm}^2$, arriving at the sample at a variable time delay, Δt , with respect to the probe. The experimental time, energy and angular resolution were better than 200 fs, 50 meV and 0.2°, respectively. The samples were cleaved *in situ* at a base pressure of $2 \cdot 10^{-10}$ mbar at room temperature, and kept at a temperature of 100-110 K during the measurement.

Figures 1(a)-(f) provide an overview of the heterostructure terminations and their respective electronic dispersions around the Γ -point of the Brillouin zone, measured at equilibrium conditions before optical excitation ($\Delta t < 0$) and during the initial moments of the excitation ($\Delta t = 40$ fs). Fig. 1(a) presents the SL MnBi_2Te_4 structure which can be thought of as a QL with an intercalated Mn-Te bilayer, introducing a plane of unpaired spins. Non-trivial topology in this system derives from its Te *5p* valence band (VB) and Bi *6p* conduction band (CB) which undergo band inversion due to spin-orbit coupling (SOC).²⁰ The dispersion before excitation at $\Delta t < 0$ in Fig. 1(d) shows intense bands within 200 meV below the Fermi level, E_F , revealing that the crystals are strongly electron-doped.²¹ We identify the ARPES intensity as being composed of bulk conduction bands (BCBs) in addition to a set of bands that are known to exhibit quasi-2D behavior.^{16,17} During excitation we observe that the bands crossing E_F become occupied up to 200 meV above E_F with high intensity in the quasi-2D bands that consist of two crossing parabolas. These features have previously been attributed to a Rashba-like spin splitting,¹⁷ suggesting a significant non-equilibrium occupation of spin-polarized carriers in this system. The topological surface state (TSS) in the bulk band gap indicated in Fig. 1(d) is characterized by a linear dispersion and is anticipated to exhibit an exchange gap below the Néel temperature.^{6,15} We do not resolve

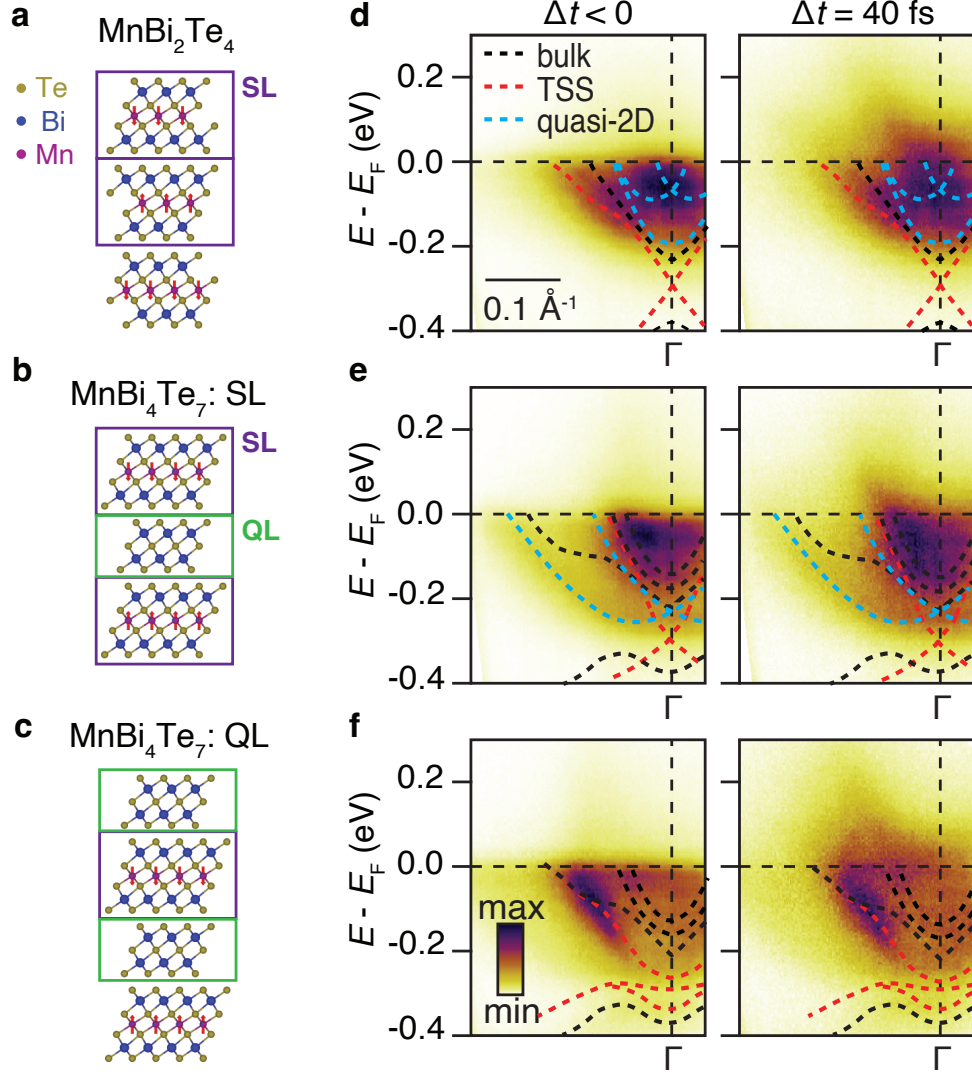


Figure 1: Overview of crystal structure and dispersion of magnetic van der Waals materials MnBi₂Te₄ and MnBi₄Te₇. (a)-(c) Layered crystal structures of (a) MnBi₂Te₄ and (b)-(c) MnBi₄Te₇ with a septuple (SL) or quintuple (QL) layer exposed at the surface. The red arrows indicate spins on the Mn atoms. (d)-(f) Photoemission intensity of the structures sketched in the same row in (a)-(c) before the arrival of the pump pulse ($\Delta t < 0$) and in the initial stage of excitation ($\Delta t = 40$ fs) with a laser fluence of $280 \mu\text{J}/\text{cm}^2$. The spectra were collected around the Γ -point of the Brillouin zone. The overlaid dashed black, red and blue dispersion lines and the noted character of the bands are based on previous high-resolution ARPES studies of the same surfaces^{7,8,15-20}

intensity from the TSS here due to the low cross section compared with the CB states at our probe polarization and photon energy.¹⁶

In MnBi₄Te₇, SL and QL units are alternating as sketched in Figs. 1(b)-(c). Cleaving the

bulk crystal can expose either of these terminations, which exhibit distinct surface electronic structures, as shown in Figs. 1(e)-(f). Both terminations exhibit a similar level of electron-doping as MnBi_2Te_4 , leading to dominant photoemission intensity from BCB states around E_F . The SL termination supports quasi-2D Rashba-like spin states that are illustrated by dashed blue parabolic bands in Fig. 1(e).^{18,19} Photoexcitation leads to dominant intensity along the BCB states and only a faint signal above E_F around these quasi-2D bands. We note that the TSS in the SL termination is a single ungapped Dirac cone,^{8,18} whereas the nature of TSS in the QL termination remains debated, with calculations showing a gapped state due to the hybridization with the underlying SL,¹⁸ but some ARPES measurements indicating a vanishing gap.^{7,8} For all surfaces the optical excitation primarily leads to a redistribution of carriers between occupied and unoccupied conduction band states. No changes in the TSS or the bulk band gaps are revealed within the resolution of our measurements.

We proceed to evaluate the detailed energy-, momentum- and time-dependent evolution of the photoexcited carriers across the three surfaces as presented in Figure 2. Panel (a) shows the photoemission intensity difference between the excited state spectrum taken 40 fs after the arrival of the pump pulse and an average of the equilibrium spectrum measured at $\Delta t < 0$. The red (blue) regions correspond to the gain (loss) of the photoemission signal, and can be interpreted as excited electron (hole) populations. From the difference spectrum of MnBi_2Te_4 we are able to see a distinct excitation of electrons above the quasi-2D bands with a Rashba-like splitting, while the excited holes are distributed across the continuum of BCB states. In contrast, both SL and QL terminations of MnBi_4Te_7 exhibit strong excitation signals from electrons mainly in regions above the BCB states.

The time-dependence of the electron (hole) dynamics in the BCB and quasi-2D states is examined by integrating the intensity within an energy- and k -window of 40 meV and 0.03 \AA^{-1} , respectively, centered ± 40 meV above (below) E_F . These integration regions are placed at different k -values for electrons and holes in order to track the intensity difference in distinct BCB and quasi-2D bands. Fig. 2(b) presents the resulting time-dependent intensity

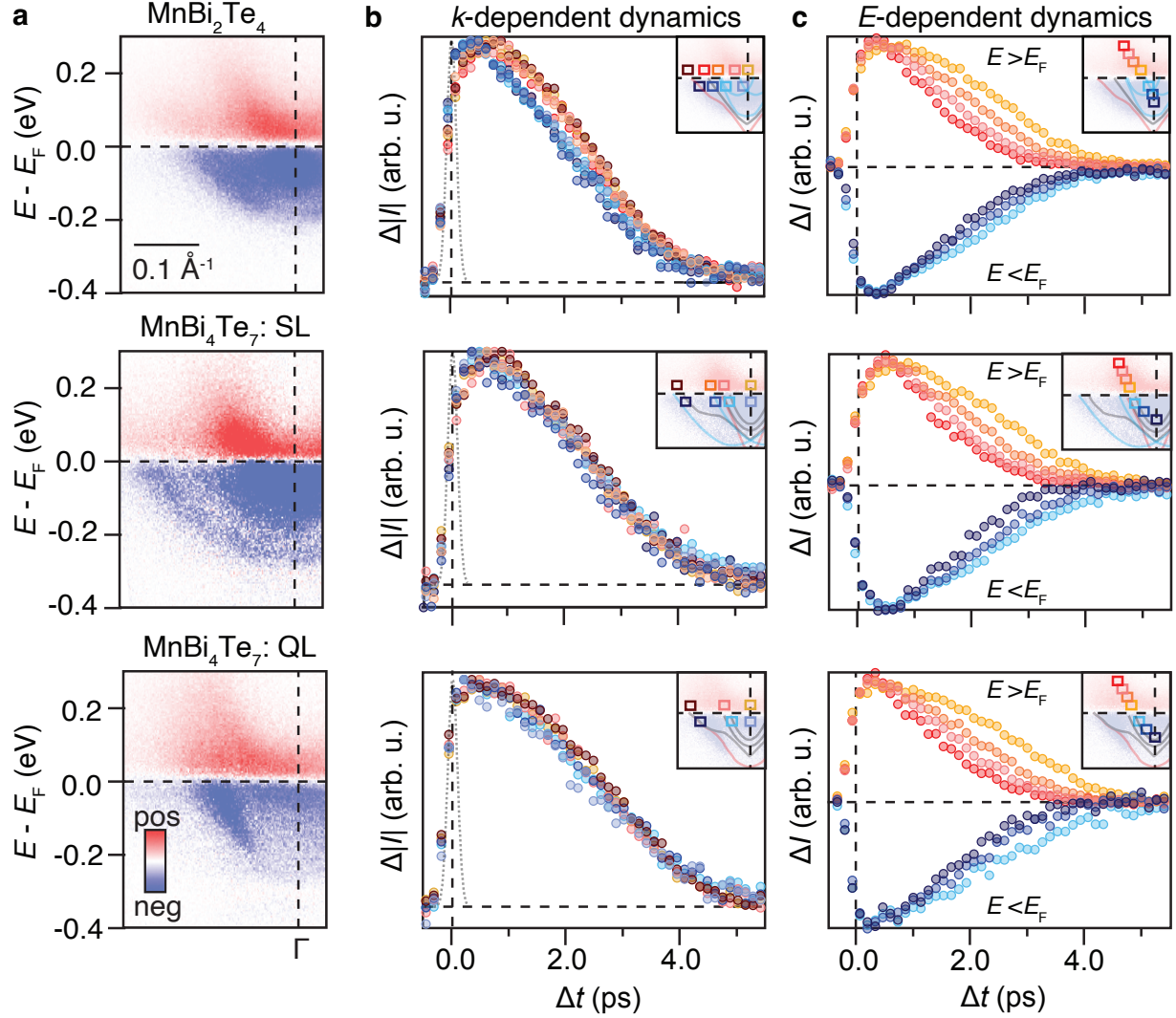


Figure 2: Energy-, momentum- and time-dependent dynamics of MnBi_2Te_4 and MnBi_4Te_7 . (a) Intensity difference spectra of MnBi_2Te_4 and MnBi_4Te_7 with SL and QL terminations obtained by subtracting an average of the equilibrium spectrum measured at $\Delta t < 0$ from the excited state signal at $\Delta t = 40$ fs. (b) Absolute values of the normalised intensity difference integrated within the (E, k) -regions demarcated by correspondingly coloured boxes in the insets, measured for different time delays. The integration regions are placed symmetrically ± 40 meV with respect to E_F in order to determine the dynamics of excited holes and electrons. (c) Normalised time-dependent intensity difference integrated within (E, k) -regions demarcated by the coloured boxes centered at varying energies in the insets, placed along the most intense band. The measurements were performed with a laser fluence of $280 \mu\text{J}/\text{cm}^2$.

around E_F for electrons, represented by red, orange and brown circles, as well as holes, represented by light and dark blue circles that are color-coded according to the integration regions in the insets. For all surfaces, the intensity due to excited carriers initially matches

the pump-probe cross-correlation integral (see dashed peak in Fig. 2(b)). The increase in the signal then slows down before reaching a short plateau which is followed by a decay back to equilibrium that is achieved around 5 ps after the excitation.

In MnBi_2Te_4 , the intensity difference corresponding to holes at -40 meV reaches its maximum at $\Delta t \approx 0.2$ ps. For the electrons at 40 meV, the maximum excitation density is achieved significantly later, at $\Delta t \approx 0.8$ ps. This electron-hole asymmetry in the dynamics diminishes in the SL termination of MnBi_4Te_7 and is absent in the QL termination where both excited electron and hole populations reach a maximum at $\Delta t \approx 0.2$ ps. The pronounced delay between the peak of electron and hole populations in MnBi_2Te_4 is attributed to the main excitation signal above E_F stemming primarily from occupation of quasi-2D bands whereas the signal below E_F is juxtaposed with the BCB continuum. Holes in the occupied part of the BCB are generated via direct optical transitions into unoccupied CB states that are resonant with the 1.55 eV pulse energy and then redistribute via efficient intra- and interband Auger processes, faster than our time resolution. The quasi-2D states above E_F are primarily filled via interband charge transfer from the initially occupied bulk states, causing a delay in the peak of the corresponding excited state population. Similar quasi-2D dynamics contributes to the intensity above E_F in the SL termination of MnBi_4Te_7 , however the prevalent BCB states diminish the effect. In the QL termination the excited state signal above E_F derives entirely from BCB states, leading to fully symmetric electron-hole dynamics deriving from identical inter- and intralayer charge redistribution processes.

The E -dependent decay dynamics is determined by inspecting the intensity difference integrated in (E, k) -regions following the band with strongest excitation signal as shown in Fig. 2(c), as demarcated by color-coded boxes in the inset. The behavior is qualitatively similar across the three systems, as in all cases the signal furthest from E_F rapidly increases during excitation and then decays exponentially while the transient population of the states closer to E_F builds up more slowly. This behavior is consistent with a cascading of intra-band scattering processes from higher-lying states.^{22,23} The slower decay dynamics of excited

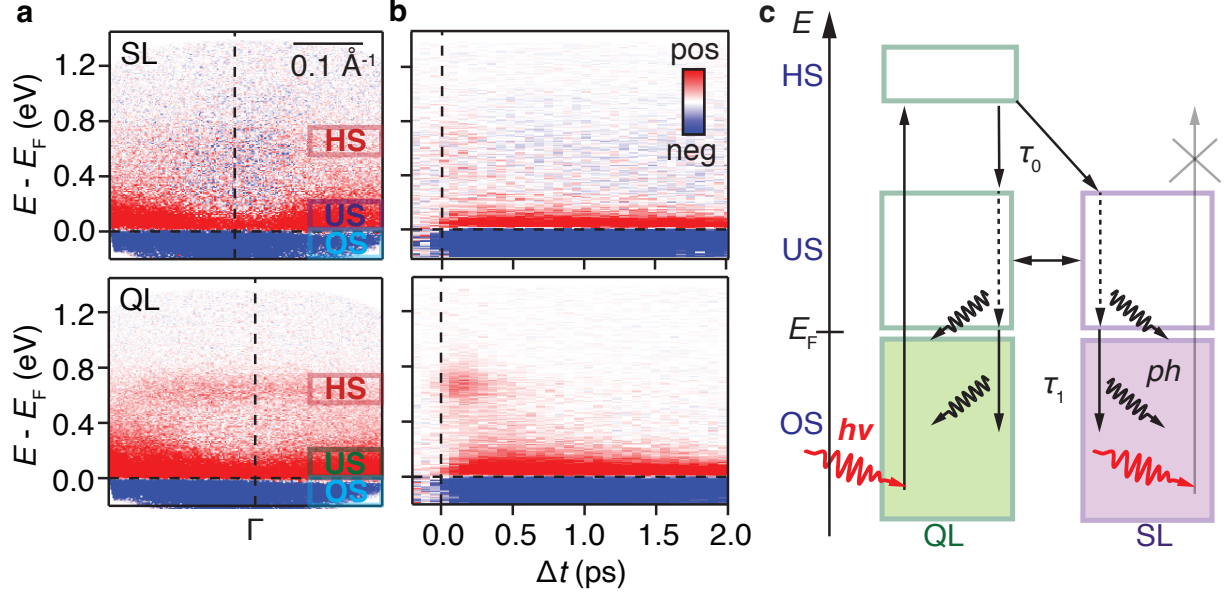


Figure 3: Intra- and interband dynamics in the van der Waals heterostructure MnBi_4Te_7 . (a) Intensity difference spectra of SL and QL terminations of MnBi_4Te_7 obtained by subtracting an average of the equilibrium spectrum measured at $\Delta t < 0$ from the excited state signal at $\Delta t = 40$ fs. (b) Energy-distribution curves (EDCs) extracted at Γ as a function of time delay for SL (top) and QL (bottom) terminations. (c) Model of interband (solid straight arrows) and intraband (dashed straight arrows) charge transfer and phonon relaxation (wiggled arrows labeled as ph) processes in the QL and SL layers of the van der Waals heterostructure initiated by the optical excitation. The high-lying states, the unoccupied states and the occupied states of the CB around E_F are labeled as HS, US and OS, respectively, as indicated by boxes in (a).

electrons and holes close to E_F is driven by the evolution of the electronic temperature and associated Fermi-Dirac distribution after excitation when a quasi-thermal equilibrium is attained.²⁴

Having established the time-dependent dynamics in states at different E - and k -regions of the excited state signal across MnBi_2Te_4 and both MnBi_4Te_7 surface terminations, we are now in a position to disentangle the layer-dependent contributions to the dynamics of the van der Waals stacked MnBi_2Te_4 and Bi_2Te_3 layers of MnBi_4Te_7 . In Figure 3(a) we inspect the transient occupation of both terminations in a wider energy window in order to determine where the initially excited electrons are generated. The QL spectrum is characterized by a strong excitation signal 0.7 eV above E_F while no states are present in this region in the

SL termination. These signals are consistent with spatially-resolved pump-probe ARPES spectra obtained on the two terminations using a micro-focused beam.¹² In analogy with Bi₂Te₃, the shallow excited band may be a surface resonance in the projected bulk band gap.²⁵

Time-dependent energy distribution curves (EDCs) at Γ , displayed in Fig. 3(b), reveal that the band at 0.7 eV in the QL is rapidly depleted while the electron and hole signals grow in the states closer to E_F in both the QL and SL. Note that the optical pump affects the electron dynamics within many layers but surface-sensitive ARPES probes primarily the first layer. We therefore propose that the initial optical excitation generates electrons in the high-lying states (HS) of the QLs in the van der Waals stack via direct transitions from the initially occupied states (OS).^{22,23} Carriers are then extracted to the unoccupied states (US) above E_F in both the QL and SL via interband charge transfer with a timescale given by τ_0 . The cascade of intraband scattering discussed above in connection with Fig. 2(c) then results in excited carriers trickling down these states and finally recombining with holes via electron-phonon coupling on a timescale labeled as τ_1 . Our model is summarised schematically in Fig. 3(c).

The optical tunability of inter- and intralayer charge transfer and phonon relaxation between QL and SL layers of MnBi₄Te₇ is demonstrated in Figure 4. We analyze the (E, k) -integrated intensity difference in the initially unoccupied states within 70 meV of E_F as a function of laser fluence and consider separately the rise part of the signal in Fig. 4(a) and the decay part on a logarithmic intensity scale in Fig. 4(b). The initial increase of the signal in Fig. 4(a) is highly fluence-dependent in the SL, exhibiting a significantly slower timescale with decreasing fluence, whereas the QL rise signal is faster and less sensitive to the fluence. In all cases, the rising part of the signal is well-described by a fit to a sigmoid function given by $(1 + \exp(2.35\Delta t/\tau_0))^{-1}$, providing an estimate of the charge transfer time τ_0 . After the initial increase in intensity, the excited state population enters a plateau region. This occurs due to the competition between the charge being transferred from the

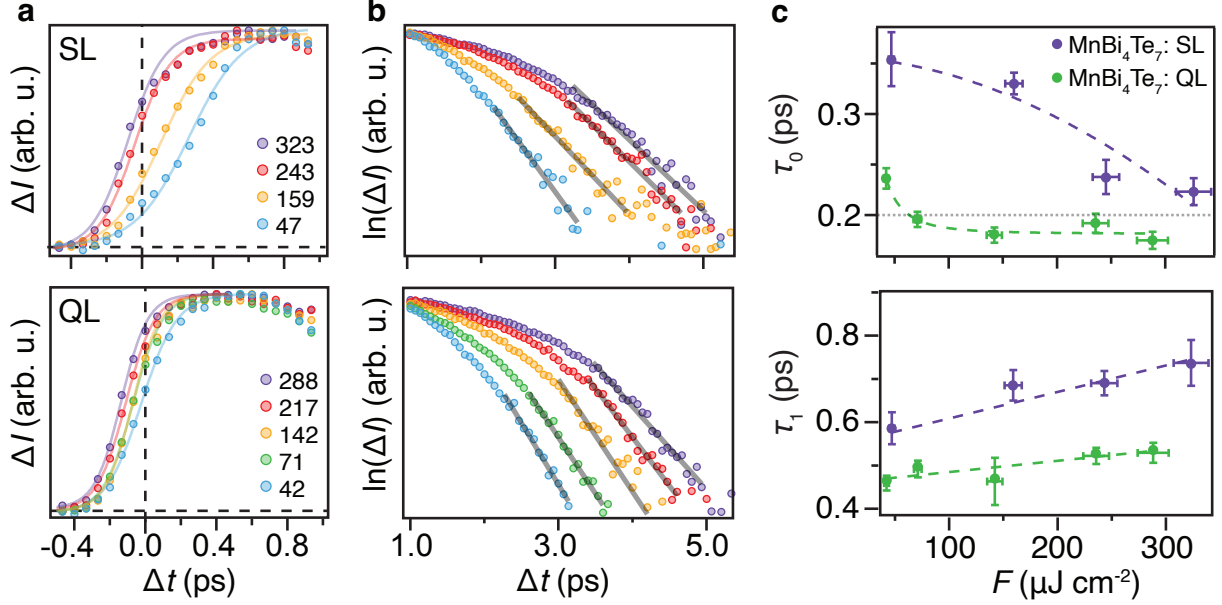


Figure 4: Charge transfer and phonon relaxation in MnBi₄Te₇. (a)-(b) (E, k) -integrated intensity difference from 0 to 70 meV above E_F and from -0.2 to 0.2 \AA^{-1} for SL and QL terminations of MnBi₄Te₇. Each data set was acquired with the fluence stated in (a) in units of $\mu\text{J}/\text{cm}^2$. In (a) we examine the rising edge of the signal (circles), representing the filling of unoccupied states above E_F , and fit a sigmoid function (curves) to extract the timescale τ_0 of the filling. In (b) we analyze the decay part of the signal on a logarithmic intensity scale and perform exponential fits (lines) to extract the phonon relaxation timescale τ_1 . (c) Extracted timescales from (a)-(b) as a function of laser fluence. Dashed curves provide a guide to the eye. Dotted gray line indicates the time resolution in this experiment.

high-lying state in the QL into unoccupied states around E_F in both the SL and QL and their subsequent recombination with holes. Finally, when the rate of refilling becomes slower than the electron-hole recombination processes, the transient occupation diminishes exponentially as shown in Fig. 4(b). We quantify the timescale τ_1 of this process via the slope of a linear fit to the logarithm of the trace in Fig. 4(b).

The extracted fluence dependence of τ_0 and τ_1 is shown in Fig. 4(c). The growth rate of the population in the SL reaches a maximum of $\tau_0 = 0.35$ ps at a low fluence of $47 \mu\text{J}/\text{cm}^2$, such that the population reaches its peak around $\Delta t = 0.80$ ps. This is substantially delayed compared to the peak being reached around $\Delta t = 0.40$ ps for $\tau_0 = 0.22$ ps at a high fluence of $323 \mu\text{J}/\text{cm}^2$. As we are considering the population in an energy range immediately above E_F , the rise time is strongly affected by interlayer charge transfer from the excited carriers

in the high lying state in the QL. For low fluence, the intralayer filling of states from the high lying state to near the Fermi level is more favourable than the interlayer charge transfer to the SL CB. Therefore the filling rate of the SL CB is slower for low excitation densities. For high excitation density, on the other hand, a large initial population is generated in the QL, thereby removing this bottleneck effect. For the QL termination, τ_0 exhibits a less dramatic fluence-dependence and merely reflects the efficiency of intralayer interband scattering.

Finally, the decay time τ_1 provides information on electron-hole recombination mediated by energy transfer to phonons.²³ The relaxation dynamics extracted in Fig. 4(c) are notably faster for QL than SL, suggesting that intralayer phonons play a dominant role in the scattering processes, in line with a substantially weakened out-of-plane interlayer vibrational interaction in the heterostructure²⁶ in comparison to its non-magnetic counterpart Bi_2Te_3 .²⁷ In all cases, the decay constant increases with applied fluence, indicating that the electron-phonon coupling becomes less efficient with a larger population of excited carriers. This trend can be explained by increased screening of the electron-phonon interaction by the photoinduced charge carriers.²⁸

In conclusion, we have determined the ultrafast charge carrier dynamics of intrinsic magnetic topological insulator van der Waals heterostructures MnBi_2Te_4 and MnBi_4Te_7 . The out-of-equilibrium distribution of excited carriers exhibit distinct dynamics in quasi-2D bands that host spin-polarized carriers in MnBi_2Te_4 , suggesting that optical pulses can be used as a tuning knob to control the magnetic properties of the system on ultrafast timescales. In MnBi_4Te_7 the dynamics is strongly affected by interlayer interactions between the Bi_2Te_3 quintuple layers and the MnBi_2Te_4 septuple layers. Direct optical excitation with a 1.55 eV laser pulse leads to a transient population of carriers in the Bi_2Te_3 layers. These excited carriers are then extracted via interband and interlayer scattering into conduction band states around the Fermi energy within the Bi_2Te_3 and in the adjacent MnBi_2Te_4 layers, respectively. In the regime of low laser fluence, the charge transfer processes into the MnBi_2Te_4 layers exhibit a bottleneck, opening the possibility to optically control the population of spin-

polarized carriers in the magnetic layers of the van der Waals stack. Furthermore, as the subsequent electron-phonon mediated relaxation is less efficient in the magnetic MnBi_2Te_4 compared to the non-magnetic Bi_2Te_3 layers it might be feasible to optically modify the magnetic properties of the heterostructure when designing spintronic and optoelectronic devices with layers of MnBi_2Te_4 .

Acknowledgement

We gratefully acknowledge funding from VILLUM FONDEN through the Young Investigator Program (Grant. No. 15375), Villum Investigator Program (Grant. No. 25931) and the Centre of Excellence for Dirac Materials (Grant. No. 11744), and the Danish Council for Independent Research, Natural Sciences under the Sapere Aude program (Grant No. DFF-9064-00057B). Work at Advanced Institute for Materials Research has benefited from support of WPI-AIMR, JSPS KAKENHI Basic Science A (18H03858), New Science (18H04473 and 20H04623), and Tohoku University FRiD program.

References

- (1) Jin, C.; Ma, E. Y.; Karni, O.; Regan, E. C.; Wang, F.; Heinz, T. F. Ultrafast dynamics in van der Waals heterostructures. *Nature Nanotechnology* **2018**, *13*, 994–1003.
- (2) Hong, X.; Kim, J.; Shi, S.-F.; Zhang, Y.; Jin, C.; Sun, Y.; Tongay, S.; Wu, J.; Zhang, Y.; Wang, F. Ultrafast charge transfer in atomically thin MoS_2/WS_2 heterostructures. *Nature Nanotechnology* **2014**, *9*, 682–686.
- (3) Zheng, Q.; Saidi, W. A.; Xie, Y.; Lan, Z.; Prezhdov, O. V.; Petek, H.; Zhao, J. Phonon-Assisted Ultrafast Charge Transfer at van der Waals Heterostructure Interface. *Nano Letters* **2017**, *17*, 6435–6442.

- (4) Yujun, D.; Yijun, Y.; Zhu, S. M.; Zhongxun, G.; Zihan, X.; Jing, W.; Hui, C. X.; Yuanbo, Z. Quantum anomalous Hall effect in intrinsic magnetic topological insulator MnBi₂Te₄. *Science* **2020**, *367*, 895–900.
- (5) Liu, C.; Wang, Y.; Li, H.; Wu, Y.; Li, Y.; Li, J.; He, K.; Xu, Y.; Zhang, J.; Wang, Y. Robust axion insulator and Chern insulator phases in a two-dimensional antiferromagnetic topological insulator. *Nature Materials* **2020**, *19*, 522–527.
- (6) Deng, H.; Chen, Z.; Wołoś, A.; Konczykowski, M.; Sobczak, K.; Sitnicka, J.; Fedorchenko, I. V.; Borysiuk, J.; Heider, T.; Pluciński, Ł.; Park, K.; Georgescu, A. B.; Cano, J.; Krusin-Elbaum, L. High-temperature quantum anomalous Hall regime in a MnBi₂Te₄/Bi₂Te₃ superlattice. *Nature Physics* **2021**, *17*, 36–42.
- (7) Xu, L. et al. Persistent surface states with diminishing gap in MnBi₂Te₄/Bi₂Te₃ superlattice antiferromagnetic topological insulator. *Science Bulletin* **2020**, *65*, 2086–2093.
- (8) Hu, Y.; Xu, L.; Shi, M.; Luo, A.; Peng, S.; Wang, Z. Y.; Ying, J. J.; Wu, T.; Liu, Z. K.; Zhang, C. F.; Chen, Y. L.; Xu, G.; Chen, X.-H.; He, J.-F. Universal gapless Dirac cone and tunable topological states in (MnBi₂Te₄)_m(Bi₂Te₃)_n heterostructures. *Phys. Rev. B* **2020**, *101*, 161113.
- (9) Otrokov, M. M.; Menshchikova, T. V.; Vergniory, M. G.; Rusinov, I. P.; Yu Viazovskaya, A.; Koroteev, Y. M.; Bihlmayer, G.; Ernst, A.; Echenique, P. M.; Arnau, A.; Chulkov, E. V. Highly-ordered wide bandgap materials for quantized anomalous Hall and magnetoelectric effects. *2D Materials* **2017**, *4*, 25082.
- (10) Sun, H.; Xia, B.; Chen, Z.; Zhang, Y.; Liu, P.; Yao, Q.; Tang, H.; Zhao, Y.; Xu, H.; Liu, Q. Rational Design Principles of the Quantum Anomalous Hall Effect in Superlattice-like Magnetic Topological Insulators. *Phys. Rev. Lett.* **2019**, *123*, 096401.
- (11) Jiaheng, L.; Yang, L.; Shiqiao, D.; Zun, W.; Bing-Lin, G.; Shou-Cheng, Z.; Ke, H.;

- Wenhui, D.; Yong, X. Intrinsic magnetic topological insulators in van der Waals layered MnBi₂Te₄-family materials. *Science Advances* **2019**, *5*, eaaw5685.
- (12) Yan, C.; Green, E.; Fukumori, R.; Protic, N.; Lee, S. H.; Fernandez-Mulligan, S.; Raja, R.; Erdakos, R.; Mao, Z.; Yang, S. An integrated quantum material testbed with multi-resolution photoemission spectroscopy. *Review of Scientific Instruments* **2021**, *92*, 113907.
- (13) Nevola, D.; Li, H. X.; Yan, J.-Q.; Moore, R. G.; Lee, H.-N.; Miao, H.; Johnson, P. D. Coexistence of Surface Ferromagnetism and a Gapless Topological State in MnBi₂Te₄. *Phys. Rev. Lett.* **2020**, *125*, 117205.
- (14) Zhong, H.; Bao, C.; Wang, H.; Li, J.; Yin, Z.; Xu, Y.; Duan, W.; Xia, T.-L.; Zhou, S. Light-Tunable Surface State and Hybridization Gap in Magnetic Topological Insulator MnBi₂Te₄. *Nano Letters* **2021**, *21*, 6080–6086.
- (15) Chen, Y. J. et al. Topological Electronic Structure and Its Temperature Evolution in Antiferromagnetic Topological Insulator MnBi₂Te₄. *Phys. Rev. X* **2019**, *9*, 041040.
- (16) Yan, C.; Fernandez-Mulligan, S.; Mei, R.; Lee, S. H.; Protic, N.; Fukumori, R.; Yan, B.; Liu, C.; Mao, Z.; Yang, S. Origins of electronic bands in the antiferromagnetic topological insulator MnBi₂Te₄. *Phys. Rev. B* **2021**, *104*, L041102.
- (17) Estyunin, D. A.; Klimovskikh, I. I.; Shikin, A. M.; Schwier, E. F.; Otrokov, M. M.; Kimura, A.; Kumar, S.; Filnov, S. O.; Aliev, Z. S.; Babanly, M. B.; Chulkov, E. V. Signatures of temperature driven antiferromagnetic transition in the electronic structure of topological insulator MnBi₂Te₄. *APL Materials* **2020**, *8*, 21105.
- (18) Wu, X. et al. Distinct Topological Surface States on the Two Terminations of MnBi₄Te₇. *Phys. Rev. X* **2020**, *10*, 031013.

- (19) Vidal, R. C. et al. Orbital Complexity in Intrinsic Magnetic Topological Insulators MnBi_4Te_7 and $\text{MnBi}_6\text{Te}_{10}$. *Phys. Rev. Lett.* **2021**, *126*, 176403.
- (20) Li, H. et al. Dirac Surface States in Intrinsic Magnetic Topological Insulators EuSn_2As_2 and $\text{MnBi}_{2n}\text{Te}_{3n+1}$. *Phys. Rev. X* **2019**, *9*, 041039.
- (21) Chemical Aspects of the Candidate Antiferromagnetic Topological Insulator MnBi_2Te_4 . *Chemistry of Materials* **2019**, *31*, 2795–2806.
- (22) Hajlaoui, M.; Papalazarou, E.; Mauchain, J.; Lantz, G.; Moisan, N.; Boschetto, D.; Jiang, Z.; Miotkowski, I.; Chen, Y. P.; Taleb-Ibrahimi, A.; Perfetti, L.; Marsi, M. Ultrafast Surface Carrier Dynamics in the Topological Insulator Bi_2Te_3 . *Nano Letters* **2012**, *12*, 3532–3536.
- (23) Sobota, J. A.; Yang, S.; Analytis, J. G.; Chen, Y. L.; Fisher, I. R.; Kirchmann, P. S.; Shen, Z.-X. Ultrafast Optical Excitation of a Persistent Surface-State Population in the Topological Insulator Bi_2Se_3 . *Phys. Rev. Lett.* **2012**, *108*, 117403.
- (24) Crepaldi, A.; Ressel, B.; Cilento, F.; Zacchigna, M.; Grazioli, C.; Berger, H.; Bugnon, P.; Kern, K.; Grioni, M.; Parmigiani, F. Ultrafast photodoping and effective Fermi-Dirac distribution of the Dirac particles in Bi_2Se_3 . *Phys. Rev. B* **2012**, *86*, 205133.
- (25) Sánchez-Barriga, J.; Battiato, M.; Krivenkov, M.; Golias, E.; Varykhalov, A.; Romualdi, A.; Yashina, L. V.; Minár, J.; Kornilov, O.; Ebert, H.; Held, K.; Braun, J. Sub-picosecond spin dynamics of excited states in the topological insulator Bi_2Te_3 . *Phys. Rev. B* **2017**, *95*, 125405.
- (26) Cho, Y.; Kang, J. H.; Liang, L.; Taylor, M.; Kong, X.; Ghosh, S.; Kargar, F.; Hu, C.; Balandin, A. A.; Puretzky, A. A.; Ni, N.; Wong, C. W. Phonon modes and Raman signatures of $\text{MnBi}_{2n}\text{Te}_{3n+1}$ ($n = 1, 2, 3, 4$) magnetic topological heterostructures. *Phys. Rev. Research* **2022**, *4*, 013108.

- (27) Liang, L.; Zhang, J.; Sumpter, B. G.; Tan, Q.-H.; Tan, P.-H.; Meunier, V. Low-Frequency Shear and Layer-Breathing Modes in Raman Scattering of Two-Dimensional Materials. *ACS Nano* **2017**, *11*, 11777–11802.
- (28) Heid, R.; Sklyadneva, I. Y.; Chulkov, E. V. Electron-phonon coupling in topological surface states: The role of polar optical modes. *Scientific Reports* **2017**, *7*, 1095.